Collective dynamics of model microorganisms with chemotactic signaling

Johannes Taktikos,[1] Vasily Zaburdaev,[1,2] and Holger Stark[1]
[1]*Institut für Theoretische Physik, Technische Universität Berlin, Hardenbergstraße 36, 10623 Berlin, Germany*
[2]*School of Engineering and Applied Science, Harvard University, 29 Oxford Street, Cambridge, Massachusetts 02138, USA*
(Received 25 January 2012; published 1 May 2012)

Various microorganisms use chemotaxis for signaling among individuals—a common strategy for communication that is responsible for the formation of microcolonies. We model the microorganisms as autochemotactic active random walkers and describe them by an appropriate Langevin dynamics. It consists of rotational diffusion of the walker's velocity direction and a deterministic torque that aligns the velocity direction along the gradient of a self-generated chemical field. To account for finite size, each microorganism is treated as a soft disk. Its velocity is modified when it overlaps with other walkers according to a linear force-velocity relation and a harmonic repulsion force. We analyze two-walker collisions by presenting typical trajectories and by determining a state diagram that distinguishes between free walker, metastable, and bounded cluster states. We mention an analogy to Kramer's escape problem. Finally, we investigate relevant properties of many-walker systems and describe characteristics of cluster formation in unbounded geometry and in confinement.

DOI: 10.1103/PhysRevE.85.051901 PACS number(s): 87.18.Ed, 45.50.−j, 87.17.Jj

I. INTRODUCTION

The self-organization of identical units into complex time- and space-dependent structures appears as one of the most fascinating and common features in nature [1]. Aristotle's understanding after which the whole is greater than the sum of its parts, also holds for biological systems. Many microorganisms form aggregates and ultimately constitute a multicellular organism that offers optimal living conditions for the cell community [2]. Important paradigms of multicellular communities are biofilms, formed by various species, such as *B. subtilis*, *P. aeruginosa*, and *E. coli* [3,4]. To coordinate growth, motion, and biochemical activities, microorganisms interact and communicate with each other by physical and chemical means. For instance, direct cell to cell contact is a typical physical interaction [5,6], whereas chemotaxis and quorum sensing represent the most prominent examples for signaling mechanisms with the help of chemicals [7,8].

Chemotaxis denotes the directed motion of microorganisms along the gradient of a chemical substance called chemoattractant [9]. Many cells such as the bacteria *E. coli* and *S. typhimurium* or the amoeba *Dictyostelium discoideum* (*Dicty* in short) produce chemoattractants themselves under certain living conditions and use it for chemotactic signaling [10]. In the following we refer to it as autochemotaxis. It provides an important means for microorganisms to communicate with and to attract each other.

A central aspect of current research on chemotaxis is the collective dynamics of chemotactic cells [11–17]. Further research concentrates on understanding internal signaling pathways on the biochemical level [18–21] and on elucidating mathematical features of chemotaxis models [22]. Numerous studies more related to nonequilibrium statistical physics examine active particle systems with a particular focus on clustering and collective motion [23–28]. In the present publication we aim to present and analyze a generic model for autochemotaxis of identical model microorganisms and study, in particular, the formation of clusters and their properties.

In our previous work we have introduced a model for the dynamics of a single autochemotactic walker [29]. Here we give the formerly point-like walker a finite extent and regard it as soft disk which is repelled by other walkers as soon as the disks overlap. Inspired by experimental results of Miyata *et al.* [30], we assume a linear relation between the velocity of the walker and the force acting on it. For simplicity, the repulsive force between two walkers is harmonic. For two autochemotactic walkers we present a state diagram where we identify free walker, metastable, and bounded cluster states in terms of the chemotactic coupling strength, one of our relevant parameters. Apart from ensemble averaged quantities, such as the mean lifetime of a two-walker cluster and the size and asymmetry of larger aggregates, we also show typical trajectories of the model microorganisms. When the chemotactic field is not sufficiently strong, some of the two-walker clusters in the metastable state break up during simulation time. We investigate this situation in detail and compare it to Kramers' escape problem. At the end, we qualitatively study some aspects of many-walker systems. Walkers can form metastable or hot clusters that dissolve in time. Stable clusters relax exponentially toward their stationary circular shape after some disturbance. Several of these microcolonies coalesce into one bigger cluster. Experiments with cells, such as granulocytes or *Dicty*, have shown that clustering requires a minimal cell density [31,32]. By tuning our model parameters in confined geometry, we confirm this experimentally observed clustering transition.

The article is organized as follows. In Sec. II we first introduce our model of autochemotactic active walkers (Sec. II A), treat collisions between walkers by modeling them as soft disks (Sec. II B), relate our parameters to biological quantities, and introduce a rescaled version of our model (Sec. II C). We study the properties of two-walker and many-walker systems in Secs. III and IV, respectively. Finally, we summarize our results in Sec. V.

II. THE MODEL

A. Autochemotactic active walkers

We model motile microorganisms that communicate via autochemotaxis as active Brownian walkers using a Langevin

equation. In a previous publication [29] we have motivated our approach in detail and just summarize it here. We consider a system of m identical walkers that move on a planar surface with velocities $\mathbf{v}_i(t)$ $(i = 1,\ldots,m)$. The observation that for various cell types fluctuations in speed and direction of motion decouple, suggests to express the velocity vectors in polar coordinates [33]. Furthermore, we keep the speed of isolated particles constant, $|\mathbf{v}_i(t)| = v$, so that the velocity of particle i becomes

$$\mathbf{v}_i(t) = v\mathbf{e}_i(t) = v\begin{pmatrix}\cos\varphi_i(t)\\ \sin\varphi_i(t)\end{pmatrix}. \tag{1}$$

The unit vector $\mathbf{e}_i(t)$ gives an intrinsic direction along which isolated microorganisms move. When they collide, their velocities do not necessarily have to be parallel to $\mathbf{e}_i(t)$, as explained in Sec. II B [34]. The walker's trajectory $\mathbf{r}_i(t)$ is obtained by integrating $\frac{d}{dt}\mathbf{r}_i(t) = \mathbf{v}_i(t)$.

Each walker emits a chemical substance with a constant production rate h. The chemical diffuses in the plane with diffusion coefficient D_c and is degraded by the environment at a constant decay rate k. The resulting reaction diffusion equation for the chemical's concentration $c(\mathbf{r},t)$ thus reads

$$\partial_t\, c(\mathbf{r},t) = D_c\nabla^2 c(\mathbf{r},t) - kc(\mathbf{r},t) + h\sum_{i=1}^{m}\delta[\mathbf{r}-\mathbf{r}_i(t)], \tag{2}$$

where ∇^2 denotes the two-dimensional Laplacian.

To account for chemotaxis we define the chemotactic field $\mathbf{E}(\mathbf{r},t) = \kappa\nabla c(\mathbf{r},t)$ and introduce a torque $\mathbf{E}\times\mathbf{e}_i$ that tries to align the walker's intrinsic direction $\mathbf{e}_i(t)$ along $\mathbf{E}$. In the following we assume the coupling strength or chemotactic sensitivity κ to be constant [35]. Positive κ represents attractive chemotaxis in response to a chemoattractant, negative κ means repulsive chemotaxis due to a chemorepellent. We formulate the Langevin equation for the intrinsic direction of motion in the overdamped limit. It contains the deterministic chemotactic torque and a stochastic torque:

$$\frac{d\varphi_i(t)}{dt} = -\frac{1}{\gamma_R}\,[\mathbf{E}(\mathbf{r}_i(t),t)\times\mathbf{e}_i(t)]_z + \sqrt{2q_\varphi}\,\Gamma_i(t). \tag{3}$$

The cross product is oriented perpendicular to the plane along the z axis and $\gamma_R > 0$ is the rotational friction coefficient. As usual, $q_\varphi > 0$ denotes the strength of the Gaussian white noise $\Gamma_i(t)$ characterized by a zero mean $\langle\Gamma_i(t)\rangle = 0$ and the time correlation function $\langle\Gamma_i(t)\Gamma_j(t')\rangle = \delta_{ij}\delta(t-t')$. The noise term represents all stochastic torques acting on the walker. In contrast to ordinary Brownian motion, it also includes nonthermal contributions.

We solve Eq. (2) with the help of its Green function and then determine the chemotactic field at the particle's position $\mathbf{r}_i(t)$, $\mathbf{E} = \mathbf{E}(\mathbf{r}_i(t),t)$, which enters in Eq. (3):

$$\mathbf{E} = -\frac{\kappa h}{8\pi D_c^2}\int_0^{t-\tau_{\rm del}} dt'\,\frac{e^{-k(t-t')}}{(t-t')^2} \times\sum_{j=1}^{m}[\mathbf{r}_i(t)-\mathbf{r}_j(t')]\exp\left(-\frac{[\mathbf{r}_i(t)-\mathbf{r}_j(t')]^2}{4D_c(t-t')}\right). \tag{4}$$

Here we assume that the walkers start to emit their chemical substance at $t = 0$. Note that the concentration gradient in Eq. (4) has been derived in a more general form by Grima in Ref. [36]. The delay time $\tau_{\rm del} > 0$ regularizes the integral. It means that a walker reacts to its own emitted chemical only after a short delay. The integral representation of $\mathbf{E}(\mathbf{r}_i(t),t)$ reveals the non-Markovian property of the chemotactic interaction since the history of all trajectories contributes to the current value of $\mathbf{E}(\mathbf{r}_i(t),t)$.

B. Collisions of autochemotactic walkers

So far we have described how autochemotactic walkers interact by the chemotactic field which they create themselves. However, real microorganisms are not point-like objects and if they collide with each other, their velocities change. It is known that the shape of bacteria plays a significant role for how they cluster and the resulting collective motion (see, for example, Ref. [24]). Here we are interested in clustering as a pure result of autochemotactic signaling. Therefore, instead of introducing the specific shape of the cell body, we view an autochemotactic walker in two dimensions as a circular disk of radius a whose center moves with velocity $\mathbf{v}_i(t) = v\mathbf{e}_i(t)$. When they touch each other, they experience some repulsive force which then alters their velocities. In the following we describe how we implement the collisions between autochemotactic walkers.

When two walkers move against each other in a central collision, the repulsive force will slow them down until they both come to a halt at a stall force $F_{\rm st}$, while still trying to walk against each other. For example, for the parasitic bacterium *Mycoplasma mobile* the relation between velocity and applied force has been measured by Miyata *et al.* [30]. They found that the bacterium's gliding speed decreased linearly with force until it became zero at the applied stall force. We will use this linear velocity-force relation for our autochemotactic walkers as indicated by the solid line in Fig. 2. Each walker has an intrinsic direction $\mathbf{e}_i$ along which it walks with a speed v. During a collision with walker j, the unit vector $\mathbf{e}_i$ does not have to be parallel to the connecting line of walkers i and j (see Fig. 1). Normal to this line, the motion of the walkers is not hindered, and $\mathbf{v}_i^\perp$ is just the normal velocity component of $v\mathbf{e}_i$. However, the parallel velocity component $\mathbf{v}_i^\parallel = -v_i^\parallel\mathbf{e}_{ij}$ is slowed down by the collision so that the walker's momentary velocity $\mathbf{v}_i = \mathbf{v}_i^\parallel + \mathbf{v}_i^\perp$ deviates from $v\mathbf{e}_i$. As Fig. 2 illustrates, we assume that at a given collision angle γ between $\mathbf{e}_i$ and the connecting line, the velocity-force relation for $v_i^\parallel$ has the same slope as for the central collision. So, the parallel component as a function of the central force F_{ij} becomes

$$v_i^\parallel = -v\,\frac{F_{ij}}{F_{\rm st}} + v\cos\gamma. \tag{5}$$

In particular, the stall force for an oblique collision is smaller than for a central encounter. Note that a negative $v_i^\parallel$ means that walker i moves away from walker j. For example, when $\mathbf{e}_i$ changes its direction from a central ($\gamma = 0$) to an oblique ($\gamma \neq 0$) collision, the repulsive force F_{ij} from particle j might be strong enough that it not just stops walker i, but also reverses its parallel velocity $\mathbf{v}_i^\parallel$.

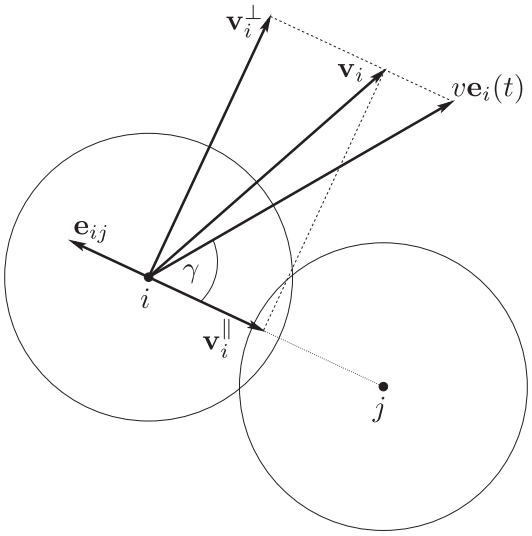

FIG. 1. Two chemotactic walkers of radius a collide. Whereas the velocity component $\mathbf{v}_i^\perp$ normal to the connecting line agrees with the normal component of the free velocity $v\mathbf{e}_i$, the parallel velocity component $\mathbf{v}_i^\parallel$ along the connecting line decreases according to a linear velocity-force relation illustrated in Fig. 2. The angle between $\mathbf{e}_i$ and the connecting line is γ and $\mathbf{e}_{ij}$ is a unit vector that points from walker j to i.

For simplicity we assume that the repulsive force $\mathbf{F}_{ij}$ is harmonic and only acts when the two disks of the walkers overlap:

$$\mathbf{F}_{ij} = \begin{cases} F_0\left(1-\frac{r_{ij}}{2a}\right)\mathbf{e}_{ij}, & r_{ij} \leqslant 2a, \\ 0, & r_{ij} > 2a. \end{cases} \tag{6}$$

Here r_{ij} is the distance between the centers of disk i and j and $F_0 > 0$ is a measure for the strength of repulsion. The force law (6) was successfully applied to model the rigidity-loss transition in foams [37]. An alternative to Eq. (6) would be a Hertzian contact force [38]. However, we do not expect large changes of the results presented below since the only purpose of Eq. (6) is to introduce some finite extension of the autochemotactic walkers.

We can now write down the velocity of walker i, $\mathbf{v}_i = -v_i^\parallel \mathbf{e}_{ij} + \mathbf{v}_i^\perp$, both during a collision ($r_{ij} < 2a$) and when it is well separated from other walkers ($r_{ij} > 2a$):

$$\mathbf{v}_i = \begin{cases} v\mathbf{e}_i + v\,\frac{1-\frac{r_{ij}}{2a}}{1-\frac{r_{st}}{2a}}\,\mathbf{e}_{ij}, & r_{ij} \leqslant 2a, \\ v\mathbf{e}_i, & r_{ij} > 2a. \end{cases} \tag{7}$$

To arrive at the upper line we have used $v\mathbf{e}_i = -v\cos\gamma\,\mathbf{e}_{ij} + \mathbf{v}_i^\perp$ together with Eqs. (5) and (6). We have also introduced the stall distance r_{st} where two walkers come to a halt during a central collision. Setting $F_{st} = F_{ij}(r_{st})$, Eq. (6) gives $r_{st}/2a = 1 - F_{st}/F_0$. To account for the softness of microorganisms during collisions, we choose typical values for $r_{st}/(2a)$ between 0.8 and 0.95 throughout our work. If a walker overlaps with several neighbors, the correction term in Eq. (7) is summed up over all neighbors and the upper line in Eq. (7) becomes

$$\mathbf{v}_i = v\mathbf{e}_i + v\sum_{j\neq i,\, r_{ij}\leqslant 2a} \frac{1-\frac{r_{ij}}{2a}}{1-\frac{r_{st}}{2a}}\,\mathbf{e}_{ij}. \tag{8}$$

A similar treatment of colliding active disks is found in the model of Ref. [39]; for an alternative interaction where a speed-dependent potential penalizes overlap between disks, we refer to Ref. [40]. In contrast to the cited publications, we have given a clear physical explanation for our treatment of colliding disks. It is based on a harmonic interaction potential and a linear relationship between force and velocity.

We add a final comment. In the following we make the simplifying assumption that the chemotactic substance is emitted at the disk center of each microorganism and that its diffusive spreading is not influenced by the finite extent of the autochemotactic walkers. Since the walkers or microorganisms move in a plane, the chemical can always use the third dimension to diffuse parallel to the plane. This would imply a full three-dimensional treatment for the diffusion of the chemical. Since it is more tedious and not crucial for the current considerations, we restricted ourselves to the two-dimensional case.

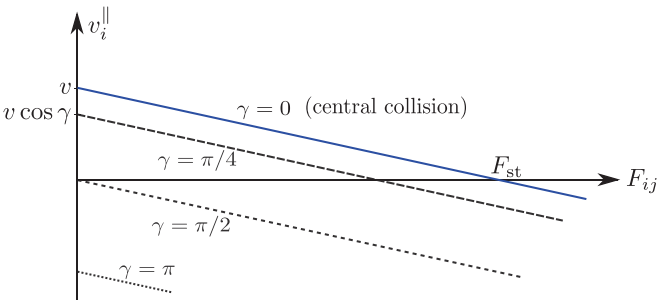

FIG. 2. (Color online) Force-velocity relation for the parallel velocity component $v_i^\parallel$ of walker i. F_{ij} is the force with which walker j acts on i. Each curve corresponds to a certain collision angle γ which is defined in Fig. 1.

C. Rescaled units and simulation parameters

We rescale lengths and velocities in our model in units of the characteristic size of a microorganism, the disk radius a, and its intrinsic speed v. Within the time unit $t_0 = a/v$, the walker moves half its body length.

For zero chemotactic field, the velocity direction diffuses on the unit circle and its directional correlations decay exponentially during the characteristic time $\tau_{rot} = q_\varphi^{-1}$, $\langle \mathbf{e}_i(t)\cdot \mathbf{e}_i(0)\rangle = \exp(-q_\varphi t)$ [29]. Hence, the walker moves on an almost straight path with persistence length $s_{per} = v\tau_{rot}$. We define the persistence number α as the persistence length in units of a:

$$\alpha = \frac{s_{per}}{a} = \frac{v}{aq_\varphi} = \frac{\tau_{rot}}{t_0}. \tag{9}$$

Since α can be rewritten as ratio of the rotational decorrelation time and the translational drift time, it was also called rotational Péclet number [41]. In the following we use α to parametrize the noise strength q_φ. The rotational diffusion of $\mathbf{e}_i(t)$ leads to a translational diffusion with coefficient $D = v^2/(2q_\varphi)$ [29]. In units of $D_0 = a^2/t_0 = av$, the diffusion coefficient reads

TABLE I. Characteristic parameters for *E. coli* and *Dicty* [13,42–46]. Chemoattractants of *E. coli* are sugars or amino acids, their decay rate k is estimated. The chemoattractant of *Dicty*, cAMP, is degraded by the enzyme phosphodiesterase with known rate k given in Refs. [13,46]. The directional correlation time $\tau_{\rm rot}$ of *E. coli* is adjusted such that $D = v^2/(2q_\varphi)$ gives the measured diffusion coefficient. It equals the duration of three run-and-tumble events. Other values are calculated from $t_0 = a/v$, $D_0 = av$, $\alpha = \tau_{\rm rot}/t_0$, and $l_c = \sqrt{D_c/k}$.

	a (μm)	v (μm/s)	t_0 (s)	D_0 (m^2/s)	$\tau_{\rm rot} = q_\varphi^{-1}$ (s)	α
E. coli	1	20	0.05	2×10^{-11}	3.3	66
Dicty	5	0.1	50	5×10^{-13}	500	10
	D (m^2/s)	D_c (m^2/s)	D/D_c	D_0/D_c	k (1/s)	l_c/a
E. coli	6.6×10^{-10}	10^{-9}	0.66	0.02	0.4	50
Dicty	2.5×10^{-12}	3×10^{-10}	0.008	0.002	0.09	11.5

$D/D_0 = \alpha/2$, that is, a larger persistence number results in enhanced diffusion.

In Table I we list characteristic values for *E. coli* and *Dicty* and their chemoattractants. Since molecules of the chemoattractant are much smaller than microorganisms, one finds for the diffusion coefficient D_c of the chemoattractant: D/D_c, $D_0/D_c \ll 1$. Based on the values from Table I, we keep the reduced decay rate $kt_0 = 0.1$ and the ratio $D_0/D_c = 0.005$ constant during all simulations. During its lifetime k^{-1} a chemoattractant molecule diffuses a typical length $l_c = \sqrt{D_c/k}$ [47]. In our simulations we have $l_c = 44.7a$. Realistic values for the persistence number α should be between 10 and 100 and we will set $\alpha = 25$ in many simulations. Finally, we introduce the dimensionless chemotactic coupling strength [48]:

$$\Lambda = \frac{\kappa h a}{D_c^2 \gamma_{\rm R}}. \tag{10}$$

We choose the delay time $\tau_{\rm del}$, introduced in Eq. (4), as small as possible and, therefore, choose it to be equal to the time step of the simulation. Moreover, a rough estimate of $\tau_{\rm del}$ justifies this procedure also from the biological perspective: As the chemoattractant is emitted at the center of our model microorganism, it takes a characteristic time t_c for the chemical to diffuse over the cell body, such that it can dock at the receptors on the surface. This time t_c should be comparable to the delay time $\tau_{\rm del}$. We use $t_c \sim a^2/D_c$ and express t_c in units of t_0 as $t_c/t_0 \sim D_0/D_c$. For $D_0/D_c = 0.005$ and a time step of $10^{-2}\, t_0$, t_c and $\tau_{\rm del}$ are thus of the same order of magnitude.

From now on we give all lengths, times, and velocities in units of a, t_0, and v, respectively. This holds in particular for all figures.

III. ANALYSIS OF THE TWO-WALKER SYSTEM

The coupled dynamics of two autochemotactic walkers is strongly influenced by the strength of their chemotactic interaction. In this section we study typical trajectories of two walkers that start close to each other and illustrate some of them in Sec. III A. In particular, it is of interest if two autochemotactic microorganisms can form stable clusters where they are bounded to each other. Without chemotactic coupling, $\Lambda = 0$, both walkers separate from each other due to translational diffusion. A small chemotactic strength Λ influences the walker's trajectories, but the chemotactic field is not strong enough to hold the particles together. For large Λ, bounded states are observed. However, they will eventually break up due to stochastic fluctuations. This is similar to Kramers' escape problem, where a particle leaves a deep potential well after an average escape time which exponentially grows with the barrier height. In Sec. III B we introduce a state diagram as a function of chemotactic strength Λ and persistence number α where we distinguish between free, metastable, and bounded walker states. In the bounded state, all the two-walker clusters stay bounded during the observation time, whereas in the metastable state for medium values of Λ, they coexist with free walkers. Finally, in Sec. III C we study the mean lifetime of a two-particle cluster in more detail and deepen the analogy to Kramers' escape problem.

A. Typical trajectories

We discuss typical trajectories that illustrate the free and bounded particle states. To generate these trajectories we put two walkers close together at an initial distance $d_0 = 2.5$ (in units of disk radius) and with random velocity directions. For small $\Lambda \ll 0.1$, the chemotactic coupling is so weak that both active Brownian walkers move independently from each other. Of course, when we chose the initial distance much larger than the range l_c of chemotactic interaction, the walkers would also simply separate in most cases. Figure 3 shows trajectories for five values of Λ and fixed persistence number $\alpha = 25$.

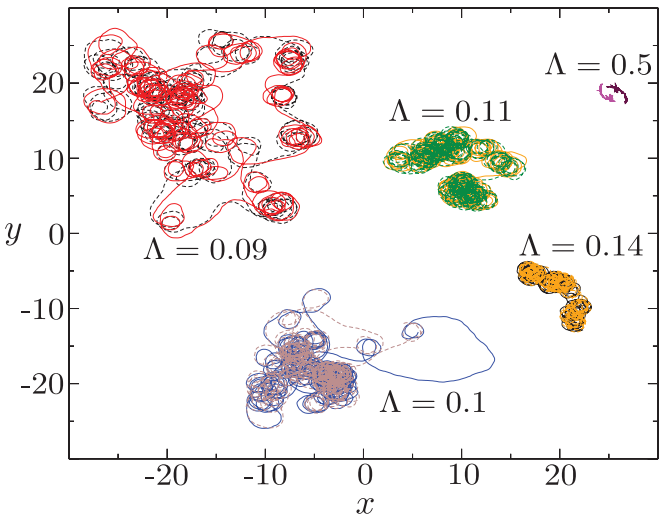

FIG. 3. (Color online) Typical pairs of trajectories of two autochemotactic walkers for fixed persistence number $\alpha = 25$ and different chemotactic strength Λ.

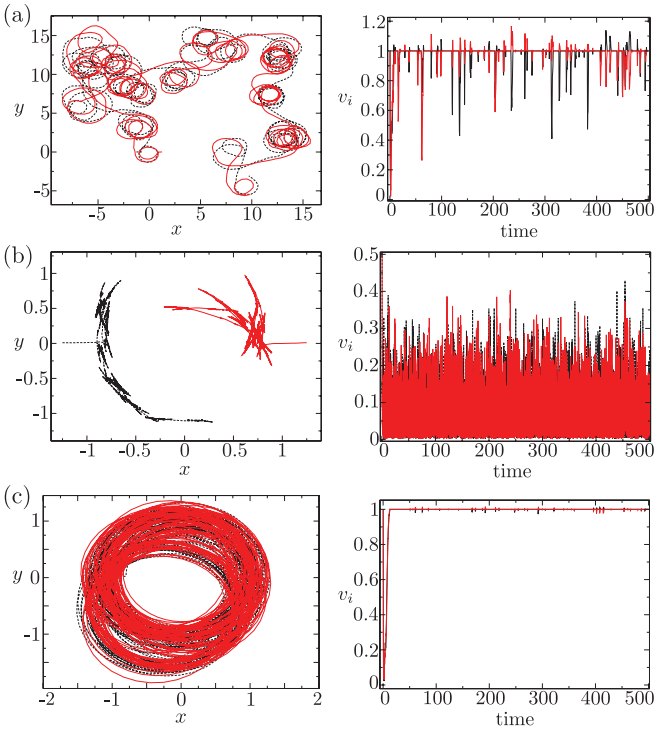

FIG. 4. (Color online) Trajectories (left column) and corresponding particle speeds v_i vs time (right column) for different parameters: (a) $\Lambda = 0.09, \alpha = 25$; (b) $\Lambda = 0.5, \alpha = 25$; (c) $\Lambda = 0.1, \alpha = 1000$. The speed $v = 1$ corresponds to free walkers without contact to other individuals.

At $\Lambda = 0.09$ and larger values, the chemotactic interaction is so strong that the walkers are bounded to each other and move strongly correlated. At $\Lambda \approx 0.1$, they circle around each other, are shortly in contact, and then separate again. Occasionally, it looks as if one active walker hunts for the second. Further increase of Λ reduces the "hunting." The walkers stop separating from each other and form a tightly bounded cluster ($\Lambda \approx 0.5$). In Fig. 4 we show closeups of the trajectories for $\Lambda = 0.09$ and 0.5, together with the speed v of the walkers. At $\Lambda = 0.09$, v varies between 1, where the walkers are not in contact with each other, and smaller values, which indicates collisions. The speed also becomes larger than one, when one walker pushes against the other. In contrast, at $\Lambda = 0.5$ the walkers are tightly bounded to each other and the speed is always below 1.

To study the influence of the persistence number α, we present trajectories for fixed $\Lambda = 0.1$ and different values of α in Fig. 5. Small α means large stochastic noise and the coupled trajectories resemble a random walk. For increasing α, the trajectories become more compact. Ultimately, the dynamics is nearly deterministic where the active walkers circle around each other with very little contact. This is clearly illustrated in Fig. 4(c).

In Fig. 3 the trajectory for $\Lambda = 0.1$ displays a big loop at the right-hand side where one walker is clearly separated from the other walker by a large distance. If such fluctuation-induced loops become too large, the cluster of two walkers breaks up which is indeed observed in simulations. So, in between tightly bounded clusters for large $\Lambda \gg 0.1$ and free walkers at

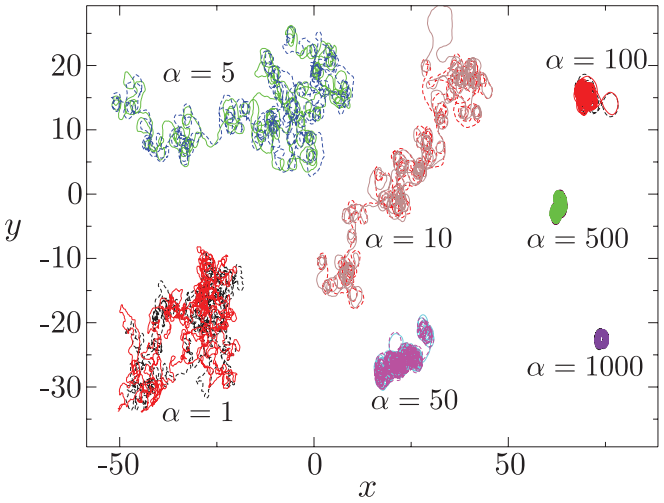

FIG. 5. (Color online) Typical pairs of trajectories of two autochemotactic walkers for fixed chemotactic strength $\Lambda = 0.1$ and different persistence number α.

$\Lambda \ll 0.1$, we find a metastable state at $\Lambda \approx 0.1$ where clusters may break up into free walkers during simulations. As already discussed, these clusters correspond to particles which escape from a potential well. In the next subsection we investigate a state diagram α versus Λ where we locate free, metastable, and bounded states in specific parameter regions. From what we said so far, it is clear that the concept of a bounded state depends on the total observation or simulation time. If this time is smaller than the mean lifetime of a cluster, then it is in the bounded state.

B. State diagram

To generate the state diagram in the parameter space persistence length α versus chemotactic strength Λ, we recorded 100 trajectories for each parameter set. The walkers started close to each other with an initial distance $d_0 = 2.5$ and opposing velocity directions with $\mathbf{r}_1(0) = (-1.25, 0.01)$, $\varphi_1(0) = 0.03$, $\mathbf{r}_2(0) = (1.25, 0.01)$, $\varphi_2(0) = \pi - 0.0001$. As a consequence they collide shortly after $t = 0$ and without noise and chemoattraction they would constitute a stable cluster for all times. We choose these deterministic initial conditions to compare only the influence of Λ and α on the cluster stability.

The simulation time was $t_{\max} = 10^4$. In real units it corresponds to typical experimental times of several hours, for example, for *Dicty* we estimate $t_{\max} = 13.9$ h using values from Table I. If all clusters of walkers for one parameter set (Λ, α) stay intact within $t_{\max}$, we refer to them as bounded state. In concrete, if the distances of the walkers at the end of each of the 100 trajectories are smaller than a characteristic length, we consider them as bounded clusters. We choose here the diffusion length $l_c = \sqrt{D_c/k} = 44.7$ of the chemical during its lifetime k^{-1} since l_c gives the range of the chemotactic interaction. However, even using characteristic lengths 10, 20, or 40 does not change the state diagram. Once walkers end up with a final distance larger than l_c at time $t_{\max} = 10^4$, they are in the free state. However, with a certain probability even noninteracting random walkers will have a distance smaller than l_c at $t_{\max}$. In the Appendix we estimate this probability to be 5% for $\alpha = 1$

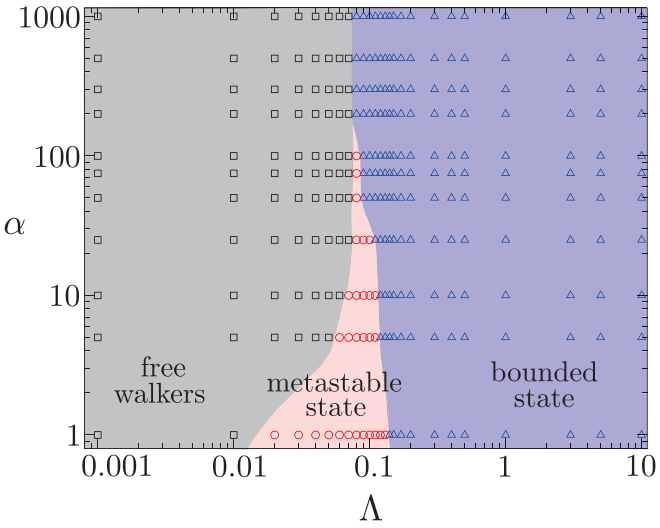

FIG. 6. (Color online) State diagram for persistence number α vs chemotactic strength Λ. The squares indicate free walkers, triangles represent walkers in the bounded state, and circles represent walkers in the metastable state.

and keep this value also for larger α. So in the state of free walkers less than 5% of them have a separation smaller than l_c. Finally, in the metastable state at least 5% of bounded clusters coexist with free walkers. The existence of three distinct states was also reported in Ref. [49] where clustering of autochemotactic walkers in one space dimension was investigated. We stress once more that the concept of bounded and metastable states always refers to the observation time $t_{\max}$ which in our case equals a reasonable experimental observation time.

Figure 6 shows the resulting state diagram. The boundary of the bounded state does hardly depend on α. Whereas for large persistence number α the almost deterministic dynamics results in a sharp transition at $\Lambda = 0.07$ between free and bounded walkers, we obtain the metastable state for decreasing α or increasing stochastic noise. This behavior is confirmed by Fig. 7, where we plot the fraction of bounded clusters versus Λ for different α. Increasing the chemotactic strength Λ, a clustering transition occurs that is smooth for small α. Therefore, stochastic noise favors the breakup of clusters, but

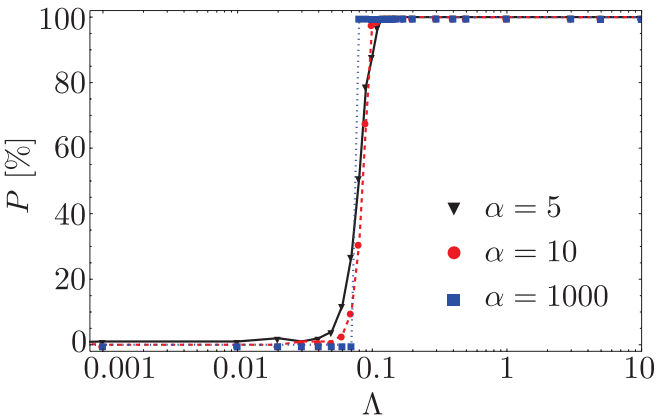

FIG. 7. (Color online) Fraction P (in %) of bounded clusters vs chemotactic strength Λ for different persistence numbers α. For larger α the sigmoidal shape converts into the step function.

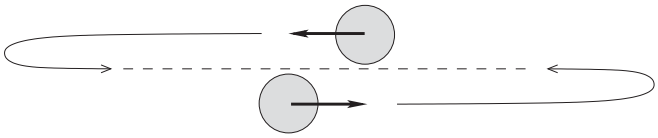

FIG. 8. To form stable clusters, active walkers separating from each other should turn around under the influence of the chemotactic field generated by both walkers.

also means a small diffusion constant, as reviewed in Sec. II C. As a result, walkers can again form clusters after breakup and thereby clusters and free walkers coexist in the metastable state. For α beyond 100, the transition becomes sharp as illustrated by the step function. Due to negligible stochastic noise, walkers only separate from each other when the intrinsic speed v is large enough to overcome the chemotactic attraction. The probability that they meet again via diffusion is small.

The clustering transition for large α occurs at a critical chemotactic strength $\Lambda \approx 0.07$. We present a rough estimate for this value. Clusters are stable when the chemotactic field generated by both walkers is strong enough to turn their velocity directions around when they move away from each other (see Fig. 8). In Ref. [29] we studied a single walker in a constant chemotactic field $\mathbf{E} = E\mathbf{e}_x$ and found that the direction of the walker relaxes towards $\mathbf{E}$ during the characteristic time $t^* = \gamma_R/E$. To form stable clusters, walkers should not separate beyond the range of the chemotactic interaction l_c or $vt^* < l_c$. Using $t^* = \gamma_R/E \propto 1/\Lambda$ we arrive in reduced units at $\Lambda > v/l_c$. With $v = 1$ and $l_c = 44.7$ this gives $\Lambda > 0.02$ which is in reasonable agreement with the simulated value 0.07.

We finish this subsection with a remark. The state diagram is insensitive to the details of the collisions between two walkers and therefore primarily determined by the chemotactic interaction. For example, if we vary the stall distance $r_{st}/(2a)$ between 0.8 and 0.95 and thereby the elasticity of the walkers, the state diagram basically does not change. This is even true when we disregard collisions of the walkers and treat them as point-like objects.

C. Mean lifetime

As already discussed, the two-walker system is in the bounded state when the cluster lifetimes exceed the simulation time. In this subsection we show that beyond the qualitative connection to Kramers' escape problem there is even a quantitative correspondence by investigating the distribution of lifetimes for parameter sets close and in the transition region between the bounded and the free-walker states. We choose the same initial conditions for two walkers as in the previous Sec. III B and define the lifetime τ of a cluster as the time when the walker separation exceeds the distance l_c for the first time.

Figure 9 plots the distribution of lifetimes at $\alpha = 100$ for $\Lambda = 0$ (inset) and $\Lambda = 0.07$. For $\Lambda = 0$ we estimate the mean lifetime $\langle\tau\rangle$ such that the mean-squared distance between the active walkers, given for example in Ref. [29], equals the characteristic distance l_c^2: $l_c^2 \approx 4\alpha^2(\langle\tau\rangle/\alpha - 1 + e^{-\langle\tau\rangle/\alpha})$. Inverting this relation for $\langle\tau\rangle$ gives

$$\langle\tau\rangle \approx \frac{l_c^2}{4\alpha} + \alpha[1 + W(-e^{-1-l_c^2/(4\alpha^2)})], \qquad (11)$$

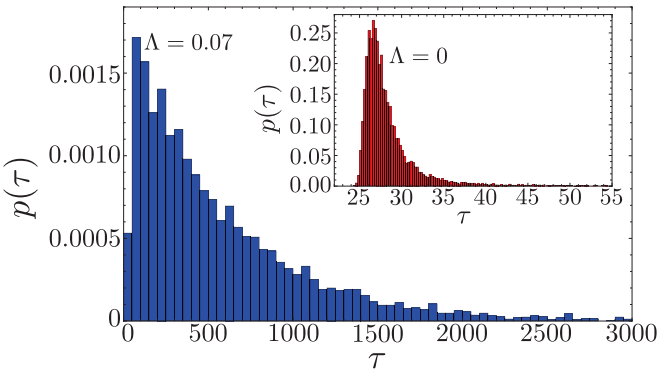

FIG. 9. (Color online) Probability distributions $p(\tau)$ of lifetimes for $\alpha = 100$ as obtained from simulations. The chemotactic strength is chosen as $\Lambda = 0.07$ and $\Lambda = 0$ (inset).

where W denotes the Lambert W function which is the inverse function of ze^z. For $\alpha = 100$ we obtain $\langle\tau\rangle = 33.3$ which agrees well with the simulated value $\langle\tau\rangle = 30.0$. This time is smaller than the directional correlation time $\alpha = \tau_{\rm rot}/t_0 = 100$ and therefore the distribution remains rather narrow. On the other hand, the distribution function $p(\tau)$ for $\Lambda = 0.07$ has a mean lifetime of $\langle\tau\rangle = 581.8$ well above α and it is very broad. In fact, we checked that the graph in Fig. 9 is well described by the inverse Gaussian distribution which gives the distribution of the first-passage times for a one-dimensional random walk [50]. The maximum of $p(\tau)$ shifts to larger τ for increasing Λ and ultimately reaches the total simulation time, meaning the system is in the bounded state.

From the lifetime distributions for $\alpha = 1$, 5, 20, 100 we determined the mean value $\langle\tau\rangle$ as a function of Λ in the region between the free walker and bounded state. Figure 10 presents two plots for $\alpha = 5$ and $\alpha = 100$. They clearly show that the mean lifetime grows exponentially in the chemotactic strength Λ, $\langle\tau\rangle \propto \exp(\Lambda/\Lambda_0)$, reminiscent of Kramers' escape rate when we identify Λ with the potential barrier. So, the mean lifetime is very sensitive to variations in Λ which also means that the value of the simulation time for defining the bounded

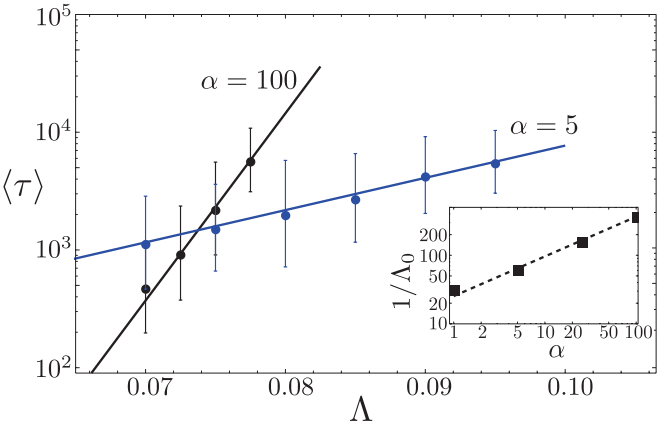

FIG. 10. (Color online) Mean lifetimes as a function of chemotactic strength Λ for $\alpha = 5$ and $\alpha = 100$. The values with error bars are obtained numerically. The solid lines are exponential fits. Inset: The slope or "inverse temperature" $1/\Lambda_0$ vs persistence number α obey the power law $1/\Lambda_0 \propto \alpha^{0.58}$.

state is not very crucial. For example, when we interpolate in Fig. 10 the straight line for $\alpha = 5$ to $\langle\tau\rangle = 10^5$, the bounded state occurs at $\Lambda \approx 0.14$ instead of $\Lambda \approx 0.104$ at a simulation time of 10^4.

In the exponential law $\langle\tau\rangle \propto \exp(\Lambda/\Lambda_0)$, $1/\Lambda_0$ plays the role of the "inverse temperature." According to the inset of Fig. 10, $1/\Lambda_0$ grows with the inverse noise strength α, as expected, following the power law $1/\Lambda_0 \propto \alpha^{0.58}$. For large α, when the system tends toward the deterministic regime, $\langle\tau\rangle$ is particularly sensitive to Λ. The transition from the free walker to the bounded state becomes more abrupt, indicating that the range of the metastable state shrinks to zero, as observed in the state diagram of Fig. 6.

IV. PROPERTIES OF A MANY-WALKER SYSTEM

In the following we study a system consisting of 50 walkers and qualitatively explore some of its properties. In particular, in Sec. IV A we address different states of the system including metastable and stable cluster states as in the two-walker case. In Sec. IV B we investigate how an initially elongated cluster relaxes toward its circular stationary shape. Then Sec. IV C demonstrates how clusters or microcolonies merge due to autochemotactic signaling. Finally, we show in Sec. IV D that in a confined geometry clustering of microorganisms occurs beyond a certain area fraction.

We briefly comment on the number of walkers in the following analysis. Though we focus on systems with 50 walkers, we observe the same qualitative features for larger systems of up to 500 walkers. Going beyond this order of magnitude increases the computational effort considerably.

A. State diagram and cluster stability

In analogy to Sec. III B we investigate the stability of clusters consisting of a large number of walkers. We place them randomly, both in position and velocity, on a square with a large area fraction of 0.5, so that they form a dense cluster and let them evolve in time. Monitoring an ensemble of roughly 10 clusters, we identify again three different states. For sufficiently large chemotactic strength Λ, all the clusters stay intact and we have the bounded cluster state. At small Λ, all the clusters dissolve and a "gas" of free chemotactic walkers results which hardly come into contact with each other. In between, a metastable state occurs. The walkers leave and join the cluster which itself fluctuates strongly. We therefore call it a "hot cluster." It can happen that the fluctuations become too large. Then, the cluster suddenly dissolves into free walkers. Figure 11 shows snapshots of such a scenario at three different times. In the supplemental material we provide the corresponding video which demonstrates how the cluster suddenly dissolves [51].

The inset of Fig. 11 shows the resulting state diagram as a function of the chemotactic strength Λ for constant $\alpha = 25$. We have already rescaled Λ by the number of walkers m. Then the metastable state is situated in the same region around $\Lambda/m \approx 0.1$ as in the two-walker case where we found $\Lambda \approx 0.1$. We roughly confirmed the scaling for $m = 50$, 100, and 500. Each walker emits the chemical and thereby increases the

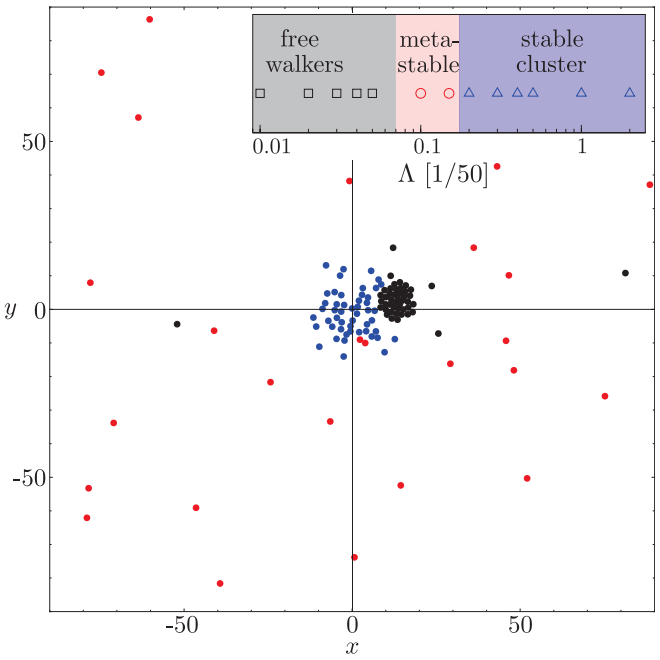

FIG. 11. (Color online) A cluster of walkers in the metastable state dissolves in time. Snapshots of the walkers at three different times: $t = 5$ [blue (dark gray), disks initially distributed on a square of side length 17.7], $t = 1000$ (black), and $t = 1500$ [red (light gray)]. Parameters are $\Lambda = 0.002$, $\alpha = 25$, and initial area fraction 0.5. Inset: State diagram recorded for $m = 50$ particles with $\alpha = 25$.

autochemotactic field which mediates an attraction between the walkers. This justifies the observed scaling.

We briefly mention the Keller-Segel model for chemotactic aggregation (see, e.g., Refs. [52,53]). In its simplest form it shows a "chemotactic collapse," where microorganisms collapse into a δ-peaked distribution when their density exceeds a critical value. Equivalently, for constant density the collapse occurs at a chemotactic strength Λ that scales as the inverse of the number m of microorganisms, in full agreement with our result. However, by taking into account the finite extent of the walkers, we prevent the unrealistic collapse and obtain stable clusters. Finally, we comment that a sufficiently high temperature, connected to the noise in the system, also prevents the chemotactic collapse as reported in Ref. [54]. Note that a modification of the classical Keller-Segel model also introduces a finite particle size [55]. Similarly, a stability analysis of the uniform density in the Keller-Segel model reveals a transition to pattern formation at a chemotactic strength that scales again as $1/m$ [12,56].

B. Relaxation dynamics of stable clusters

The stable clusters of walkers are circular when m is sufficiently large. To describe the size and shape of a walker distribution in a disturbed cluster, we introduce the gyration tensor $\mathbf{Q}$. It is defined as

$$\mathbf{Q} = \frac{1}{2m^2} \sum_{i,\,j=1}^{m} (\mathbf{r}_i - \mathbf{r}_j) \otimes (\mathbf{r}_i - \mathbf{r}_j), \tag{12}$$

where $\otimes$ specifies the dyadic product [57]. Diagonalizing $\mathbf{Q}$ yields two eigenvalues $\lambda_1 \geqslant \lambda_2 \geqslant 0$. An ensemble average over $\lambda_1 + \lambda_2$, which is the trace of $\mathbf{Q}$, gives the square of the radius of gyration, which is a measure for the size of the cluster:

$$R_g^2 = \frac{1}{2m^2} \sum_{i,\,j=1}^{m} \langle [\mathbf{r}_i(t) - \mathbf{r}_j(t)]^2 \rangle \tag{13}$$

$$= \frac{1}{m} \sum_{i=1}^{m} \langle [\mathbf{r}_i(t) - \mathbf{R}(t)]^2 \rangle. \tag{14}$$

Here we have introduced the position vector of the center of mass, $\mathbf{R} = 1/m \sum_{i=1}^{m} \mathbf{r}_i$. The cluster has a circular shape when both eigenvalues are equal, $\lambda_1 = \lambda_2$. To describe deviations from the spherical shape, we introduce the asymmetry parameter Δ_2 as the following ensemble average [58]:

$$\Delta_2 = \left\langle \frac{(\lambda_1 - \lambda_2)^2}{(\lambda_1 + \lambda_2)^2} \right\rangle. \tag{15}$$

When all walkers align along one line, $\Delta_2 = 1$.

In the following we demonstrate that at large chemotactic strength $\Lambda = 0.02$, a cluster of loosely packed walkers relaxes exponentially toward a densely packed cluster with circular shape. As Fig. 12(a) on the left demonstrates, we distribute 50 particles uniformly on an ellipse with asymmetry $\Delta_2 \approx 0.15$ and area fraction 0.5, and randomly choose the velocity directions. The picture on the right shows the densely packed cluster after relaxing into the stationary state. In Fig. 12(b) we show how the squared radius of gyration R_g^2 and the asymmetry Δ_2 smoothly relax toward the circular cluster state with $\Delta_2 \approx 0$. The ensemble average is taken over 100 different realizations of initial conditions and noise. After substracting the respective minimum values from R_g^2 and Δ_2, the intermediate parts of the curves in the semilogarithmic plots in Fig. 12(c) are nicely fit by an exponential decay with relaxation times $t_g = 2.4$ for the cluster's size and $t_a = 3.4$ for its asymmetry [see red lines in Fig. 12(c)].

Note, whereas the cluster size decreases continuously in Fig. 12(b), the asymmetry first increases due to restructuring of the cluster and then relaxes toward zero. We recorded similar curves for different persistence numbers $\alpha = 5$ and $\alpha = 100$. In our simulations the initial concentration of chemoattractant is zero. We also performed a few simulations where we initially fixed the walker positions, let the chemotactic field establish a stationary profile, and then recorded the relaxation curves for R_g^2 and Δ_2. They resemble the ones in Fig. 12(b). Finally, as expected, reducing the chemotactic strength Λ results in a weaker attraction between the walkers and thus in a less compact cluster with larger R_g^2.

The circular cluster on the right-hand side of Fig. 12(a) also illustrates that the velocity directions of the walkers point radially inwards towards the cluster center where the concentration of the chemoattractant and thereby the chemotactic attraction is largest.

C. Microcolonies merge into a central cluster

So far we have shown that a uniform distribution of chemotactic walkers at sufficiently large chemotactic strength

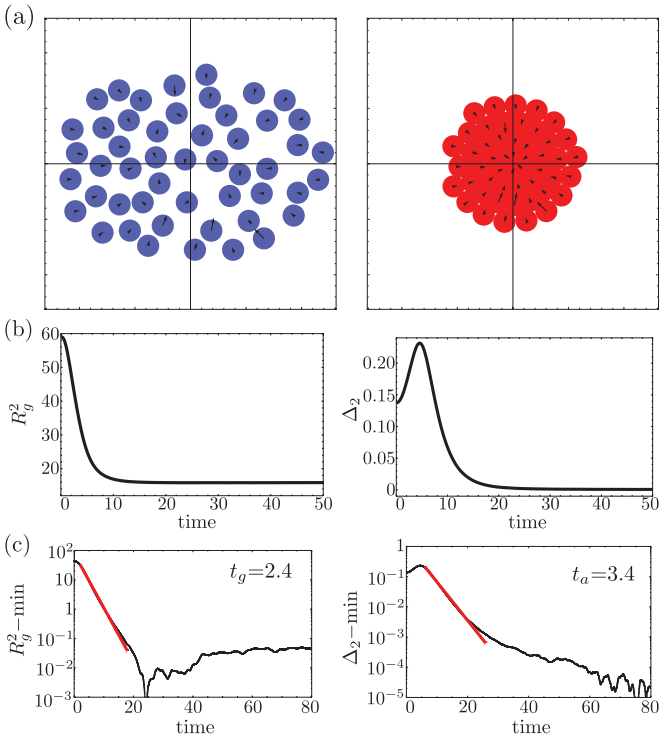

FIG. 12. (Color online) (a) The initial ellipsoidal walker distribution relaxes exponentially into a circular cluster for chemotactic strength $\Lambda = 0.02$ ($\alpha = 25$). The arrows indicate the velocity directions of the walkers. (b) Squared radius of gyration R_g^2 and asymmetry Δ_2 plotted vs time. (c) To obtain the semilogarithmic plots, the minimum values of R_g^2 and Δ_2 have been subtracted, respectively. The thick straight lines are exponential fits with respective relaxation times $t_g = 2.4$ and $t_a = 3.4$.

Λ and initial area fraction forms a stable cluster, which we view here as a microcolony. This can be interpreted as result of communication between individual cells mediated by the chemotactic field. On a higher level of aggregation, several microcolonies also interact via autochemotactic signaling and eventually merge into larger aggregates. The snapshots in Fig. 13 illustrate the scenario of four microcolonies merging into one central cluster for parameters $\Lambda = 0.02$ and $\alpha = 25$. Note that there is an analogy between the fusion of autochemotactic clusters into larger aggregates and the phenomenon of Ostwald ripening in nucleation theory, as analyzed in Refs. [28,54].

The drift of single clusters in the previous example is possible through an asymmetric arrangement of the walkers' velocity directions within the cluster which add up to the center-of-mass velocity of the cluster. Geometry is important in the cluster's drift velocity. Though the stable cluster shown in Fig. 12 looks spherical, the small but nonzero value of the asymmetry Δ_2 generates a small drift velocity and the cluster moves around. The importance of geometry and symmetry becomes already clear for small clusters. Four walkers usually pack into a rhomboid [Fig. 14(a)] with their velocity directions pointing radially inward so that it hardly moves. Clusters of five walkers pack into more asymmetric clusters, as illustrated in Fig. 14(b), and exhibit a clear drift motion. Figure 15(a)

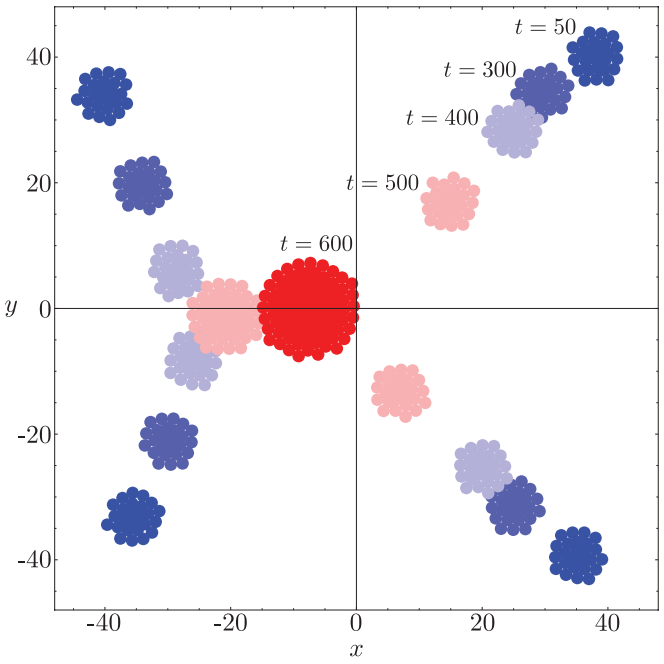

FIG. 13. (Color online) Four microcolonies, each with 25 particles, merge into a larger aggregate. The snapshots are for $t = 50$ (four blue clusters at the edges), $t = 300$, 400, 500 and $t = 600$ (single red cluster in the center). Parameters are $\Lambda = 0.02$ and $\alpha = 25$.

on the right, to be discussed in detail below, presents another example: The walkers coalesce quickly into a cluster whose center-of-mass then moves along the thin line. Even though in clusters consisting of many walkers the cluster velocity may be several order of magnitude smaller compared to the speed of a single active walker, it enables the cluster to explore its environment.

For clarification, we point out that even two initially perfectly symmetric clusters will merge into one aggregate due to strong chemotactic attraction. While drifting toward each other, the internal structure will change.

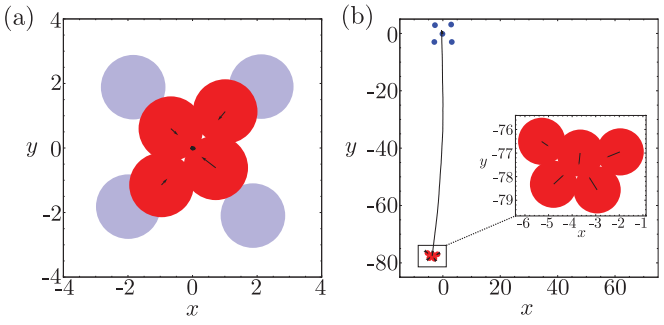

FIG. 14. (Color online) (a) A cluster of four walkers forms from an initial configuration (light blue particles at the outer positions). The cluster hardly moves since the velocities of the single walkers cancel each other. (b) A cluster of five walkers is less symmetric (see blow-up) and therefore shows a noticeable drift as its trajectory shows. Both simulations were performed for the same time $t_{\max} = 10^3$ and parameters $\Lambda = 1$, $\alpha = 25$.

D. Microorganisms in confined geometry with fixed area fraction

Clustering of microorganisms in real systems due to chemotaxis requires a minimal area fraction which is typically of the order of 5%–10% and also depends on the type of cell. At low calcium concentrations, granulocytes attract each other over small distances and form clusters of actively moving cells if the density exceeds a threshold of 150–300 cells/mm^2 [31]. If we take the diameter of a granulocyte as $2a = 20\ \mu$m and use the cell area of πa^2, the critical density corresponds to a critical area fraction of $\rho = 4.6\%$–9.2%. Aggregation of *Dicty* cells requires a minimum density of 400 cells/mm^2 [32]. With an estimate for an effective radius of $a = 5.5\ \mu$m, this threshold corresponds to $\rho = 3.8\%$.

We will now show that our model reproduces the experimental observation that clustering only occurs beyond a sufficiently large area fraction of microorganisms. By adjusting the parameters appropriately, in particular, the chemotactic strength Λ, we find clustering at an area fraction similar to experiments. We perform simulations with 50 chemotactic walkers and several area fractions $\rho = 0.01$, 0.05, and 0.1 in a circular area for which we implement a soft boundary with the help of overlapping disks [Fig. 15(a)]. They are nonmotile, nonchemotactic but repel the walkers with the harmonic force law of Eq. (6). As for the chemotactic walkers, we assume that the diffusion of the chemoattractant is not influenced by the presence of the boundary disks. Initially, the walkers are uniformly distributed over the circular area with area fraction ρ and have random velocity directions.

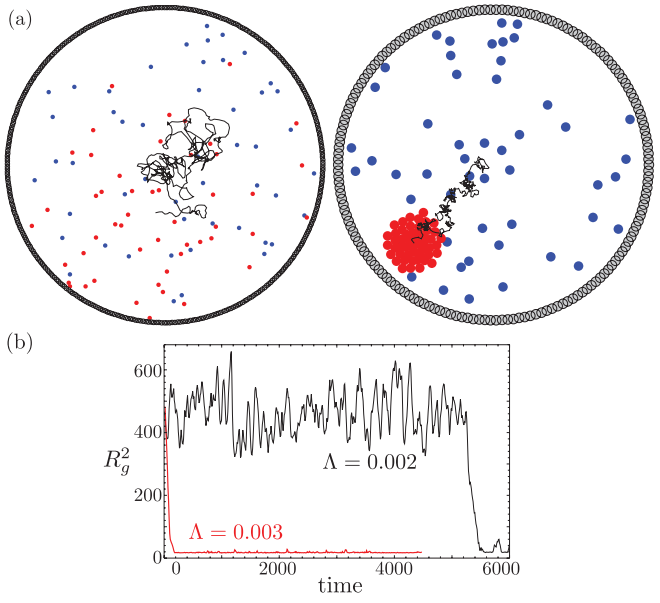

FIG. 15. (Color online) (a) Simulations of 50 walkers in a circular area with soft boundary for two area fractions ρ and constant $\Lambda = 0.003$ and $\alpha = 25$. Left: $\rho = 0.01$, right: $\rho = 0.05$. Blue (dark gray) and red (light gray) circles indicate, respectively, the initial and final positions. The thin line shows the trajectory of the center of mass of all walkers, $\mathbf{R}(t) = 1/m \sum_{i=1}^{m} \mathbf{r}_i(t)$. On the right-hand side $\mathbf{R}(t)$ coincides with the center of the cluster. (b) Squared radius of gyration R_g^2 of the walker system vs time for $\Lambda = 0.003$ and $\Lambda = 0.002$ (with the same $\alpha = 25$ and $\rho = 0.05$). Whereas the cluster with $\Lambda = 0.003$ forms shortly after the simulation is started, the walkers at $\Lambda = 0.002$ suddenly collapse into a cluster after some time.

The effective chemotactic strength Λ depends on the parameters of the self-generated chemical field and on the chemotactic sensitivity κ, but not on the density of microorganisms. It turns out by choosing, in particular, $\Lambda = 0.003$ and for example $\alpha = 25$, we are able to observe the clustering transition for experimentally relevant area fractions. Figure 15(a) shows particle distributions for two different area fractions ρ in the beginning and at the end of the simulations. For $\rho = 0.01$ the system remains in the gas state [on the left of Fig. 15(a)], whereas for $\rho = 0.05$ [on the right of Fig. 15(a)] and $\rho = 0.1$ (not shown) the walkers form a cluster in a sudden collapse shortly after the simulation starts [Fig. 15(b)]. Our model thus reproduces the experimental finding that clustering of microorganisms requires a minimal area fraction of the order of 5%. Note that a sudden collapse into a cluster also occurs for $\Lambda = 0.002$, but only after some time has passed [Fig. 15(b)].

The state diagram in Fig. 11 has been obtained for an open system where the area fraction cannot be fixed. In the future it might be interesting to determine state diagrams with specified boundary conditions that are realized in a petri dish or microfluidic devices.

V. SUMMARY

In this article we proposed a model for microorganisms that communicate via autochemotaxis. To do so, we extended our previous work on autochemotactic walkers from Ref. [29] and included a repulsive interaction between individual walkers by modeling them as soft disks. Based on a linear relationship between the harmonic repulsion force acting on a walker and its velocity, we were able to treat collisions between the autochemotactic walkers.

Already in a two-walker system, we find a rich variety of trajectories depending on the chemotactic strength Λ. They range from independent random walkers, to walkers that hunt each other, up to strongly bounded clusters where the walkers never lose contact with each other. A state diagram in terms of chemotactic coupling strength Λ and persistence number α contains the free-walker, the metastable, and the bounded state, where the latter was defined relative to the simulation time. We were able to estimate the critical chemotactic strength where the clustering transition to the bounded state occurs. To elucidate the metastable state and the transition to stable two-particle clusters, we analyzed the distribution of cluster lifetimes and showed that the mean lifetime $\langle\tau\rangle$ in the metastable regime grows exponentially in the chemotactic strength Λ, $\langle\tau\rangle \propto \exp(\Lambda/\Lambda_0)$. The effective "inverse temperature" $1/\Lambda_0$ follows a power law in the inverse noise strength α. The exponential law for $\langle\tau\rangle$ is reminiscent of Kramers' escape rate of a trapped Brownian particle from a potential well.

Many-walker systems show the same sequence of states for increasing chemotactic strength Λ. At sufficiently strong chemotactic strength, clusters or microcolonies have a circular shape. Elliptically shaped clusters relax exponentially toward the stable circular outline within a certain characteristic

relaxation time. Small asymmetries of the cluster shape result in a drift motion of the center of mass. Finally, with our model we confirmed experimental observations that clustering requires a minimal density of microorganisms. In particular, we could adjust the chemotactic strength Λ such that the clustering transition occurs around an area fraction of 5%.

In conclusion, we formulated a minimal model to mimic the essential physics of chemotaxis-induced aggregation of microorganisms. For this reason, our model does not include microscopic details of the chemotaxis sensory system. For example, our model assumes an instantaneous reaction to the chemical gradient without any threshold value for the absolute concentration. We were able to show that even within this simple model several walkers form microcolonies and that already for two interacting walkers a variety of motional patterns exists. Detailed experimental studies will help to determine the relevant region in the parameter space of our model and thereby test our predictions. Future theoretical investigations should improve the modeling for the spreading chemoattractant. In reality, it is emitted at the microorganisms' surfaces, where it also binds to receptors [13]. Especially in dense bacterial systems, the free diffusion of chemical is influenced by the presence of the microorganisms and it would be interesting to study how it influences the behavior of our model system.

ACKNOWLEDGMENTS

We thank Reinhard Vogel, Andreas Zöttl, Matthias Theves, and Carsten Beta for helpful discussions. This work was funded by the Research Training Group GRK 1558 'Nonequilibrium Collective Dynamics in Condensed Matter and Biological Systems' of the Deutsche Forschungsgemeinschaft and under DFG Grant No. ZA593/2-1 (VZ).

APPENDIX: PROBABILITY TO FIND A PARTICLE DISTANCE BELOW A GIVEN VALUE

We consider two independent, nonchemotactic walkers with constant speed v and rotational diffusion of their velocity direction. In the following we estimate the probability that the particle distance $d(t) = \sqrt{[\mathbf{r}_1(t) - \mathbf{r}_2(t)]^2}$ at time $t > 0$ is below some value R.

For large times, $\langle d^2(t)\rangle$ increases linearly in time and the "diffusion coefficient" $D_{\rm dist}$ is twice the diffusion constant D of a single walker [59]. We assume that both walkers start their random walk at the origin. For large times we thus approximate the time evolution of $\mathbf{d}(t)$ by simple two-dimensional diffusion. The corresponding diffusion coefficient $D_{\rm dist}$ is defined by $D_{\rm dist} = \lim_{t\to\infty}\langle d^2(t)\rangle/(4t)$. The solution of the diffusion equation $\partial_t P(\mathbf{r},t|\mathbf{r}_0,t_0) = D_{\rm dist}\,\nabla^2 P(\mathbf{r},t|\mathbf{r}_0,t_0)$ with initial condition $P(\mathbf{r},t_0|\mathbf{r}_0 = 0,t_0 = 0) = \delta(\mathbf{r})$ is given by

$$P(\mathbf{r},t|\mathbf{r}_0 = 0,t_0 = 0) = \frac{1}{4\pi D_{\rm dist} t}\,\exp\left(-\frac{\mathbf{r}^2}{4D_{\rm dist}t}\right). \quad \text{(A1)}$$

The probability $\mathrm{Prob}(r < R,t)$ that the particle distance r at time t is smaller than R is calculated as

$$\begin{aligned}\mathrm{Prob}(r < R,t) &= \int_0^{2\pi} d\varphi \int_0^R dr\, r\, P(r,\varphi,t)\\ &= 1 - \exp\left[-\left(\frac{R}{\sqrt{4D_{\rm dist}t}}\right)^2\right]. \quad \text{(A2)}\end{aligned}$$

This result is intuitive as $\sqrt{4D_{\rm dist}t}$ corresponds to the root of the mean-squared displacement at time t. For $R \ll \sqrt{4D_{\rm dist}t}$ the probability in Eq. (A2) vanishes, whereas for $R \gg \sqrt{4D_{\rm dist}t}$ it approaches one. In our rescaled model we have $D_{\rm dist} = 2D = \alpha$. For the simulation time $t_{\max} = 10^4$ and the critical distance $l_c = 44.7$, we obtain $\mathrm{Prob}(r < l_c, t_{\max}) = 4.9\%$ for $\alpha = 1$ and 0.5% for $\alpha = 10$. We use the former value of approximately 5% to determine the transition between free walkers and metastable states in Sec. III B.

[1] E. Ben-Jacob and H. Levine, Nature (London) **409**, 985 (2001).
[2] J. A. Shapiro, Annu. Rev. Microbiol. **52**, 81 (1998).
[3] T. Romeo, Ed., *Bacterial Biofilms*, Current Topics in Microbiology and Immunology, Vol. 322 (Springer, Berlin, 2008).
[4] E. Karunakaran, J. Mukherjee, B. Ramalingam, and C. Biggs, Appl. Microbiol. Biotechnol. **90**, 1869 (2011).
[5] D. Bray, *Cell Movements: From Molecules to Motility*, 2nd ed. (Garland Science, New York, 2001).
[6] E. Ben-Jacob, I. Cohen, and H. Levine, Adv. Phys. **49**, 395 (2000).
[7] J. Wingender, T. R. Neu, and H. C. Flemming, Eds., *Microbial Extracellular Polymeric Substances* (Springer, Berlin, 1999).
[8] C. M. Waters and B. L. Bassler, Annu. Rev. Cell Dev. Biol. **21**, 319 (2005).
[9] M. Eisenbach, *Chemotaxis*, 1st ed. (Imperial College Press, London, 2004); T. Jin and D. Hereld, Eds., *Chemotaxis: Methods and Protocols*, Methods in Molecular Biology (Springer, Berlin, 2009).
[10] N. Mittal, E. O. Budrene, M. P. Brenner, and A. van Oudenaarden, Proc. Natl. Acad. Sci. USA **100**, 13259 (2003). D. Woodward, R. Tyson, M. Myerscough, J. Murray, E. Budrene, and H. Berg, Biophys. J. **68**, 2181 (1995); K. F. Swaney, C.-H. Huang, and P. N. Devreotes, Annu. Rev. Biophys. **39**, 265 (2010).
[11] A. Sengupta, T. Kruppa, and H. Löwen, Phys. Rev. E **83**, 031914 (2011).
[12] P. Romanczuk, U. Erdmann, H. Engel, and L. Schimansky-Geier, Eur. Phys. J.: Special Topics **157**, 61 (2008).
[13] D. S. Calovi, L. G. Brunnet, and R. M. C. de Almeida, Phys. Rev. E **82**, 011909 (2010).
[14] B. M. Friedrich and F. Jülicher, Proc. Natl. Acad. Sci. USA **104**, 13256 (2007).
[15] M. Inoue and K. Kaneko, Phys. Rev. E **77**, 041916 (2008).
[16] P. M. Lushnikov, N. Chen, and M. Alber, Phys. Rev. E **78**, 061904 (2008).
[17] T. V. Kasyap and D. L. Koch, Phys. Rev. Lett. **108**, 038101 (2012).
[18] A. Celani, T. Shimizu, and M. Vergassola, J. Stat. Phys. **144**, 219 (2011).
[19] Y. V. Kalinin, L. Jiang, Y. Tu, and M. Wu, Biophys. J. **96**, 2439 (2009).

[20] F. Matthäus, M. S. Mommer, T. Curk, and J. Dobnikar, PLoS ONE **6**, e18623 (2011).

[21] M. J. Tindall, S. L. Porter, P. K. Maini, and J. P. Armitage, PLoS Comput Biol. **6**, e1000896 (2010).

[22] T. Hillen and K. Painter, J. Math. Biol. **58**, 183 (2009); M. Herrero, *Handbook of Differential Equations Evolutionary Equations*, edited by C. M. Dafermos and E. Feireisl (Elsevier, 2007), Vol. 3; D. Horstmann, I. Jahresberichte DMV **105**, 103 (2003).

[23] G. Grégoire, H. Chaté, and Y. Tu, Physica D: Nonlinear Phenom. **181**, 157 (2003).

[24] F. Peruani, A. Deutsch, and M. Bär, Phys. Rev. E **74**, 030904 (2006).

[25] F. Ginelli, F. Peruani, M. Bär, and H. Chaté, Phys. Rev. Lett. **104**, 184502 (2010).

[26] H. P. Zhang, A. Beer, E.-L. Florin, and H. L. Swinney, Proc. Natl. Acad. Sci. USA **107**, 13626 (2010).

[27] S. Henkes, Y. Fily, and M. C. Marchetti, Phys. Rev. E **84**, 040301 (2011).

[28] F. Schweitzer, *Brownian Agents and Active Particles. Collective Dynamics in the Natural and Social Sciences* (Springer, Berlin, 2003).

[29] J. Taktikos, V. Zaburdaev, and H. Stark, Phys. Rev. E **84**, 041924 (2011).

[30] M. Miyata, W. S. Ryu, and H. C. Berg, J. Bacteriol. **184**, 1827 (2002).

[31] H. Gruler, U. Dewald, and M. Eberhardt, Eur. Phys. J. B: Complex Syst. **11**, 187 (1999).

[32] P. v. Sengbusch, *Molekular- und Zellbiologie* (Springer, Berlin, 1979); *Der Schleimpilz Dictyostelium discoideum. Ein Modellorganismus zum Studium der Entstehung eines Vielzellers* [http://www.biologie.uni-hamburg.de/b-online/d27_10/27_10.htm].

[33] M. Schienbein and H. Gruler, Bull. Math. Biol. **55**, 585 (1993).

[34] Hydrodynamic interactions in bacterial suspensions also strongly reduce the correlation between the intrinsic axis and the swimming direction [60]. Furthermore, in real microorganisms $\mathbf{e}_i(t)$ does not have to be oriented along their main axis. Rod-like bacteria, for example, can also move perpendicular to their long axis [24].

[35] In general, the chemotactic sensitivity $\kappa(c)$ is a function of the concentration c [61]. In particular, microorganisms usually need a minimal concentration to detect the chemical.

[36] R. Grima, Phys. Rev. Lett. **95**, 128103 (2005).

[37] D. J. Durian, Phys. Rev. Lett. **75**, 4780 (1995).

[38] K. L. Johnson, *Contact Mechanics* (Cambridge University Press, Cambridge, 1987).

[39] B. Szabó, G. J. Szöllösi, B. Gönci, Z. Jurányi, D. Selmeczi, and T. Vicsek, Phys. Rev. E **74**, 061908 (2006).

[40] F. Peruani and G. J. Sibona, Phys. Rev. Lett. **100**, 168103 (2008).

[41] I. O. Götze and G. Gompper, Phys. Rev. E **82**, 041921 (2010).

[42] H. C. Berg, *Random Walks in Biology* (Princeton University Press, Princeton, NJ, 1993).

[43] H. C. Berg and L. Turner, Biophys. J. **58**, 919 (1990).

[44] L. Li, S. F. Norrelykke, and E. C. Cox, PLoS ONE **3**, e2093 (2008).

[45] R. G. Endres and N. S. Wingreen, Proc. Natl. Acad. Sci. USA **105**, 15749 (2008).

[46] J.-L. Martiel and A. Goldbeter, Biophys. J. **52**, 807 (1987).

[47] M. Postma, L. Bosgraaf, H. M. Loovers, and P. J. M. Van Haastert, EMBO Rep **5**, 35 (2003).

[48] Note that in Ref. [29] we used a different reduced coupling strength which is connected to the chemotactic strength used in this paper: $\Lambda = a/l_c \times \Lambda_{\text{Ref. [29]}}$.

[49] M. Inoue and K. Kaneko, Phys. Rev. E **74**, 011903 (2006).

[50] J. L. Folks and R. S. Chhikara, J. R. Stat. Soc. Ser. B **40**, 263 (1978).

[51] See Supplemental Material at http://link.aps.org/supplemental/10.1103/PhysRevE.85.051901 for the corresponding video which demonstrates how the cluster suddenly dissolves.

[52] P. H. Chavanis, Eur. Phys. J. B: Complex Syst. **57**, 391 (2007).

[53] P. M. Lushnikov, Phys. Lett. A **374**, 1678 (2010).

[54] F. Schweitzer and L. Schimansky-Geier, Physica A (Amsterdam) **206**, 359 (1994).

[55] K. J. Painter and T. Hillen, Can. Appl. Math. Q. **10**, 501 (2002).

[56] R. Tyson, S. R. Lubkin, and J. D. Murray, J. Math. Biol. **38**, 359 (1999).

[57] J. W. Cannon, J. A. Aronovitz, and P. Goldbart, J. Phys. I France **1**, 629 (1991).

[58] B. Maier and J. O. Rädler, Macromolecules **34**, 5723 (2001).

[59] This is seen by noting that $\langle \mathbf{d}^2(t) \rangle = \mathbf{d}_0^2 + 2 \times \text{MSD}_1(t)$ and the MSD_1 of a single walker reads $\text{MSD}_1(t) = \frac{2v^2}{q_\varphi^2} + (q_\varphi t - 1 + e^{-q_\varphi t})$.

[60] A. Sokolov, I. S. Aranson, J. O. Kessler, and R. E. Goldstein, Phys. Rev. Lett. **98**, 158102 (2007).

[61] M. J. Tindall, P. K. Maini, S. L. Porter, and J. P. Armitage, Bull. Math. Biol. **70**, 1570 (2008).